Building Simulation 2003

Eighth International IBPSA Conference
Eindhoven, Netherlands
August 11-14, 2003

COMPUTER SIMULATION OF THERMAL IMPACT OF AIR INFILTRATION THROUGH MULTILAYERED EXTERIOR WALLS

Chebil S.[1,2], Galanis N.[1], Zmeureanu R.[2]
[1] Université de Sherbrooke, Sherbrooke, Québec, Canada
[2] Concordia University, Montreal, Quebec, Canada

Schebil@cbs-engr.concordia.ca, Nicolas.galanis@gme.usherb.ca, Zmeur@cbs-engr.concordia.ca

ABSTRACT

Convective air circulation occurring through wall layers is frequently observed in building envelopes. Significant thermal coupling can take place between the incoming cold/warm air and the wall structure, thereby modifying the thermal performances of the envelope. This paper presents an unsteady three-dimensional numerical heat and air transfer model, which was developed to characterize the air leakage effect on the thermal performance of a complete multilayered exterior wall. The modeling for coupling between heat transfer and air infiltration is compared with the commercial software FEMLAB. The results show the substantial impact of air infiltration on the thermal performance of the wall system. Overall heat losses (by conduction and due to the infiltrated air) are evaluated depending on the airflow rates and the air leakage routes. For an airflow rate of 0.001 kg/s, the heat recovery factor varies between 7 % and 15% depending on the air flow path. The reduction of heating load at different scenarios and airflow rates reaches 8%.

INTRODUCTION

Air infiltration and exfiltration through wall layers are frequently observed in building envelopes. They are generally caused by cavities that are generated accidentally either during the installation practices and/or subsequently to material deformation. Infiltration can also occur through pores, which are part of the material composition. Most of the studies reported in the literature dealt with simplified wall systems. Anderlind (Anderlind, 1985) and Liu (Liu, 1987) considered the interaction between air flow and heat conduction and showed, based on theoretical arguments, that for "ideal diffuse walls", the heating load due to the combined effects of conduction and air leakage is substantially smaller than the sum of the conductive heat flow (in the absence of airflow) and infiltration heating load, when they are considered as two decoupled phenomena.

Powell et al. (Powell et al., 1989) reviewed several studies about the influence of the air movement on the effective thermal resistance under various conditions. The paper addressed air convection in and around insulation systems exclusively. Air infiltration through the insulation, from unconditioned to conditioned space was not covered in that study. The results indicated that the thermal insulation value of a wall might decrease and differ substantially from that which is calculated by addition of R-values of different layers, due to the air convection effects.

An experimental study was carried out by Brown et al. (Brown et al., 1993) to measure the thermal resistance of frame walls with defects in the installation of mineral fiber insulation. Through full-scale laboratory measurements, this work examined the effect of corner installation defects, natural convection across the cavities and product density, on the thermal resistance of frame walls insulated with mineral fiber insulation products. The reduction of the thermal resistance varied between 2% and 36% according to the insulation material density and air temperature.

Jones et al. (Jones et al., 1995) characterized the thermal performance of residential wall systems using a calibrated hot box with airflow induced by differential pressures. Test results revealed that air infiltration rates, as low as 0.2 l/s.m^2 could produce a 46% increase in apparent conductance.

Krarti (Krarti, 1994) presented an analytical model to characterize the air leakage effects on the heat transfer through a permeable one-layered wall. The results indicated that air infiltration and exfiltration decrease significantly the overall wall resistance. The advantages of intentionally circulating the ventilation air through building walls were also discussed. It was found that the heat recovery in dynamic walls could achieve energy savings of up to 20% of total building thermal load.

Bhattacharyya and Claridge (Bhattacharyya et al., 1995) have conducted calorimetric measurements on a stud-cavity wall specimen with measured amounts of infiltration introduced under a variety of conditions (air temperature, flow rate and cavity positions). Their results indicated that infiltration through the insulation material has a much smaller impact on the space heating load than is customarily calculated. For the measured flow rates and configurations, the

Infiltration Heat Exchange Effectiveness (IHEE) has values between 16% and 70%, which indicates that in some cases, a significant reduction of heating load could be achieved. An analytical model based on fundamental heat exchange and mass transfer principles has been also developed and validated by the experimental results.

Claridge and Liu (Claridge et al., 1996) carried out experimental work to measure in/exfiltration heat recovery with different cavity positions and airflow rates applied in an outdoor test cell. Measurements showed that the heating load due to air infiltration ranged from –55% of the conventionally calculated values to +15%, depending on the air leakage rate, the airflow direction (infiltration or exfiltration), the solar radiation, and the cavity position.
Sherman and Walker (Sherman et al., 2000) have used CFD simulations for four simplified insulation/flow path cases to investigate infiltration heat recovery and to simulate sensible heat transfer in typical envelope constructions. The studied walls are made up of a central cavity (either empty or filled with glass-fiber insulation), an exterior plywood sheathing, and an interior plywood layer. The results of the CFD simulations showed that infiltration heat recovery can have a substantial effect on the heat loss prediction, and that traditional methods may greatly over predict the infiltration load by 80% to 95% at low leakage rates, and by about 20% at high leakage rates. While the CFD simulations provided useful information for comparison purpose, the authors developed also a simplified physical model to be used by engineers and building designers when estimating the heating and cooling loads due to infiltration.

The literature review described in this paper showed that heating load due to infiltration is usually overestimated since the heat recovery effects within the exterior walls are neglected. All the studies presented above considered only simple wall configurations.

This paper presents a numerical model of transient 3-D heat and air transfer phenomena in a complete wall system to evaluate the air leakage effects on typical multilayered wall performances. The temperature profiles within the wall system and the heat flux along the inner and outer wall surfaces are analyzed to show the effect of airflow on heat transmission through actual building envelopes. Modeling the coupling between heat transfer and air infiltration is compared with the commercial software FEMLAB. Heat losses by conduction and due to the infiltrated air are evaluated in terms of the airflow rates and the infiltration path.

MODEL DESCRIPTION

The multilayered wall system presented in this work is typically used in North America. A detailed cross horizontal section is shown in Figure 1. The brick layer ❶ is followed by an air gap ❷ and plywood sheathing ❸. Then, generally comes the insulation layer ❺ standing between the vertical and horizontal wood studs ❻. The interior side of the wall is covered with a gypsum board layer ❽. When the plywood and gypsum board are not well connected with the studs (due to installation practices and/or material deformation/defects), air cavities may exist around the different interfaces. Cavity positions are described on figure 1 (layer ❹: Cav1 to Cav5; layer ❼: Cav10 to Cav14). Cavities between the stud/insulation interfaces (Cav6 to Cav9) may also be present. Eventually, a shortcut crack along the whole wall thickness could also exist (Cav0 ❾), for instance underneath the window frame.
All these cavities (Cav0 to Cav14) might be the possible leakage routes for the outside cold air when infiltration occurs.

The multilayered wall is subject to different heat transfer mechanisms:

1. Heat conduction in each material.
2. Convection and radiation on both exterior and interior sides.
3. Natural convection occurring inside the air gaps of layer ❷ and the cavities Cav0 to Cav14.
4. Radiation between the surfaces of different layers.

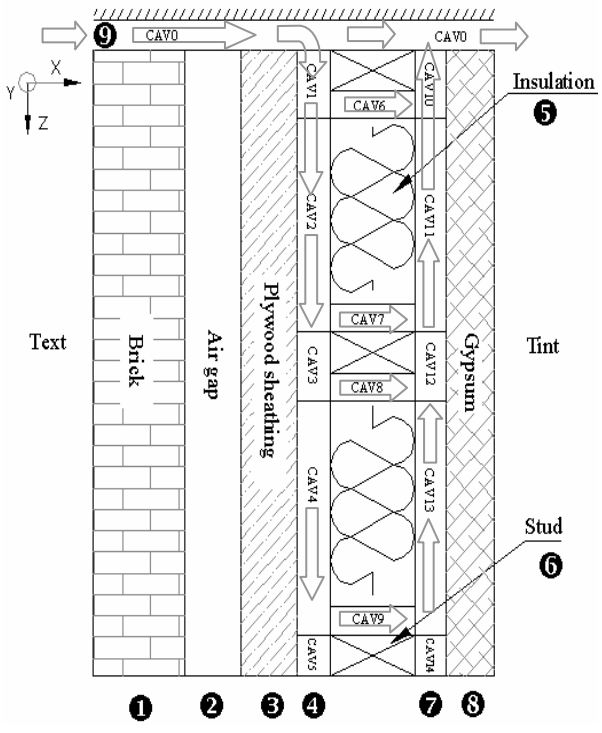

Figure 1: Horizontal section of a typical wall

5. When air flows from outside into the conditioned space (infiltration), forced convection might occur inside the cavities.
6. The top, bottom, left and right sides of the wall are subjected to constant fluxes Q_{top}, Q_{bottom}, Q_{left} and Q_{right} (W/m^2). In this paper, the adiabatic conditions are assumed on the perimeter of the considered wall ($Q_{top}= Q_{bottom}=Q_{left}=Q_{right}=0$).

The following coordinates system is selected: OX is normal to the wall, OY is vertical, and OZ is horizontal along the wall. The driving force for air leakage is a pressure differential due to wind and temperature differences between inside and outside. In this paper, the airflow rate through the wall is supposed to be constant.

METHODOLOGY

The three-dimensional heat conduction within each material is governed by Fourier's transient equation. The thermal properties are assumed to be isotropic, and independent of time and temperature.
At the inner and the outer wall surfaces (bricks and gypsum board), the combined film convection coefficients are respectively, h_{int} and h_{ext}. These coefficients are assumed constant. T_{int} is the indoor temperature and T_{ext} is the sol-air temperature at the outside surface defined as:

$$T_{ext}(t)=T_{out}(t) + I(t).\alpha/h_{ext} \quad (1)$$

Time-varying $T_{out}(t)$ and solar radiation data for a typical winter day are used for $T_{ext}(t)$ calculation. Absorptivity α of brick is taken 0.63 (ASHRAE Fundamentals, 1993).

The sol-air temperature follows generally a sinusoidal variation with a mean value, a maximum and a minimum depending on the weather data.
It is assumed that there is no perfect contact at the common boundary of two consecutive layers (e.g., brick and plywood). In that case, all air cavities described in Figure 1 are separated by air. The heat flow across each cavity is mainly affected by the nature of the boundary surfaces and the air space thickness.

When the air infiltration is not considered, heat exchange across the cavity occurs by radiation and natural convection. The radiation heat transfer between two parallel surfaces is normally calculated by a non-linear formulation in terms of the temperature and the properties of each surface. However, in order to simplify the calculations in this paper, a simplified model was used; the radiation heat flow in a "Cavity p**"** is estimated in terms of the mean temperature T_m of the boundary surfaces and the emissivity of each surface (Hollands et al. 1973):

$$h_{cavp\_rad.} = 0.227\ \varepsilon_{eff\_air}\ [(T_m + 273)/100]^3 \quad (2)$$

ε_{eff_air} is the effective emissivity calculated in terms of the emissivity of each surface. 0.227 comes from $100^3 x 4 x \sigma$, coefficient which appears when linearizing the Stefan-Boltzmann equation.

The convection heat transfer is affected by the orientation of the air space, the heat flow direction, the air and surface temperatures, and the cavity dimensions.

Hollands and Konicek (Hollands et al. 1973) found that in vertical cavities, at Grashof number $Gr_\delta \leq 8000$ the airflow consists of one large rotating cell, and in this case the heat transfer occurs essentially by conduction. As the Grashof number is increased beyond this value, the convection heat transfer becomes significant.
The correlation of Nusselt number developed by Jakob for vertical enclosed space was used to determine the convective heat coefficient "h_{cavp_conv}" (Jakob, 1949):

$$Nu_\delta = 0.18 * Gr^{0.25} *(H_{wall}/\delta)^{1/9} \quad (3)$$

The total heat transfer coefficient $hcav_p$, within a "Cavity p**",** delimited by two consecutive layers (e.g., plywood and insulation) and considering both convection and radiation heat transfer, is expressed as follows:

$$hcav_p = h_{cavp\_rad.} + h_{cavp\_conv} \quad (4)$$

For narrow air spaces, defined as those for which the product of the temperature difference (in Kelvin) and the cube of the space thickness (in millimeters) is less than 27000 (for heat flow horizontally or downward), or less than 9000 (for heat flow upward), convection is practically suppressed (ASHRAE Fundamentals, 2001). This case was not yet implemented in the numerical model.

In case when air infiltration occurs, the heat and mass transfer phenomena are coupled. The different possible airflow routes through the wall system, which are considered in this paper, are showed with arrows in Figure 1.

Assumptions:
1. Every cavity has a fixed thickness along the entire wall height.
2. The airflow coming into the wall passes through the cavity Cav0.
3. At the entrance of Cav0, the air temperature is equal to the outdoor air temperature (T_{out}).
4. No infiltration occurs in layer ❷ and in cavities 5 (Cav5) and 14 (Cav14).
5. Although the airflow can occur either through the material pores or through air cavities along insulation interfaces, in this study, only infiltration along insulation interfaces is considered.
6. Mass flow rate for each cavity is given.

In this study, the airflow in each cavity is considered to be one-dimensional: in the direction of OZ for Cav1 to Cav5 and Cav10 to Cav14, and in the direction OX for Cav0 and Cav6 to Cav9.

The simplified modeling of coupled heat and mass transfer phenomena was presented in a previous communication (Chebil et al., 2002).

In the case of laminar flow (Re<2000; covering most of the airflow rate cases occurring along wall interfaces), the following Nusselt number correlations for forced convection (Nu_f) was used (Kohonen et al., 1987):

$$Nu_f = 1.85\,(Re.Pr.D_h/H_{wall})^{1/3} \quad \text{if } Re.Pr.D_h/H_{wall} > 70$$

$$Nu_f = 7.54 \quad \text{if } Re.Pr.D_h/H_{wall} \leq 70 \qquad (5)$$

Similar to the previous case above with natural convection, when air infiltration occurs in a "Cavity n", the overall heat transfer coefficient $hcav_n$ is expressed as a sum taking into account both convection and radiation heat transfer coefficients (Equation 4 applies also to "Cavity n").

SIMULATION

A numerical model of transient 3-D heat transfer in a wall system was developed using the finite difference method. A fully implicit scheme was used for the discretization of Fourier's equation.

The Tri-Diagonal-Matrix Algorithm (TDMA) method was used to solve the above linear discretized equations. For faster convergence, OX was chosen as a line-by-line sweep direction (Patankar, 1980) .

RESULTS AND ANALYSIS

Preliminary validation

For validation purposes, the numerical estimates of transient heat flow on the inside and outside surfaces were compared with results obtained with the conduction transfer function (CTF) method. Since this method does not consider air infiltration across the wall system and is restricted to one-dimensional heat transfer, the proposed model was applied to a wall without studs, composed only of parallel layers (ASHRAE Fundamentals, 1993). This comparison was presented in previous communication (Chebil et al., 2002).

The numerical results for the case with air infiltration were compared with the results obtained with the commercial software FEMLAB (FEMLAB, 2001). This program is a Matlab-based modeling and simulating tool that solves science and engineering phenomena governed by ordinary and partial differential equations (PDE), using the finite element method. Applications combine multiphysics with built-in computer-aided design tools, including coupling between heat transfer and fluid airflow. The software is designed to simulate systems of coupled PDEs, for 1D, 2D or 3D phenomena, non-linear and time dependent.

For comparison purposes, the wall described in Figure 1 was reduced to layers ❶, ❸, ❺, ❼ and ❽. The simplified configuration is shown in Figure 2.
In that case, the airflow is supposed to go into cavity Cav1 and to leave from Cavity Cav5. The thicknesses of cavities Cav0, Cav6 to Cav9, and Cav10 to Cav14 were reduced to 1E-6 m; studs (layer ❻) were assumed to have the same thermal properties as the insulation layer ❺.

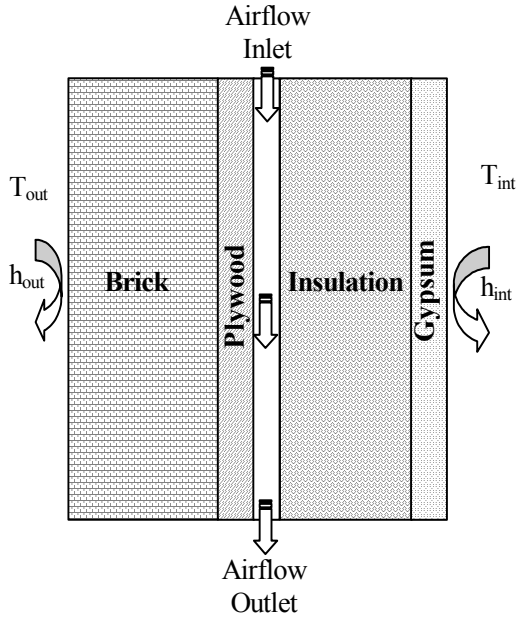

Figure 2: Simplified wall for validation with FEMLAB

A steady-state case was used. The simplified wall to model has the following characteristics (ASHRAE Fundamentals, 1993):

- 50 mm brick (K=0.72 W/m.K; k=4.5E-7 m^2/s);
- 5 mm plywood (K=0.21 W/m.K; k=1.1E-7 m^2/s);
- 3 mm air gap;
- 50 mm fibre glass (K=0.046 W/m.K; k=3.4E-6 m^2/s);
- 15 mm gypsum (K=0.727 W/m.K; k=5.4E-4 m^2/s);
- The inside and outside surface resistances h_{int} and h_{ext} are assumed 8 and 34 $W/m^2.K$, respectively;
- The wall is 2.5 m high and 1.238 m wide;
- The air is entering at -20^0C (K=0.0235 W/m.K; Cp=1009 J/kg.K; ν=11.42E-6 m^2/s; ρ=1.311 kg/ m^3; β=3.95E-3 K^{-1}).

The exterior and interior temperatures are -20^{0}C and +20^{0}C, respectively. Three different airflow rates were considered: 0.001, 0.005 and 0.01 kg/s. The numerical results presented in Figure 3 show a good agreement with the FEMLAB simulation. Air temperature through the cavity estimated by the model is about 0.5K higher than the FEMLAB prediction.

Several variables influence the heat exchange between the infiltrated airflow and the wall structure. The most significant parameters are flow rate and air leakage route (Krarti, 1994). These are considered in

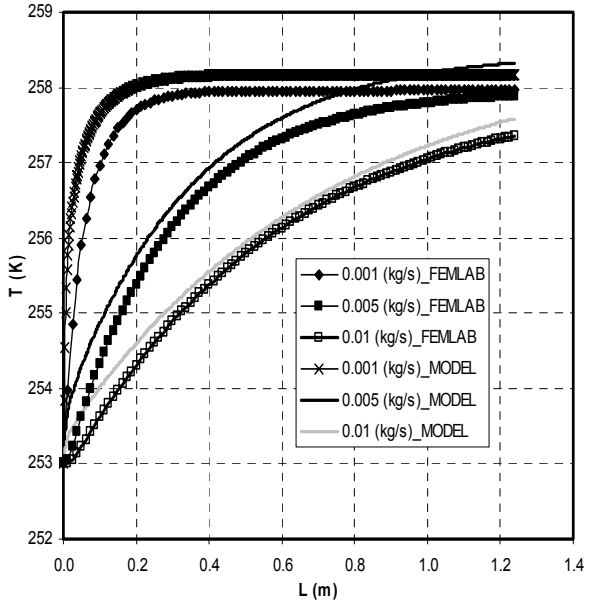

Figure 3: Air temperature through the cavity: numerical versus FEMLAB results

the following sections.

Wall performance analysis: impact of air leakage route

For the rest of this study, the typical wall is composed of the following layers with the same thermal properties as before (Figure 1):

- 100 mm brick;
- 25 mm air gap (❷);
- 12 mm plywood;
- Three wood studs (140x38 mm): two studs are installed on the perimeter of the wall, while the third is in the middle of the wall (❻ in Figure 1). The distance between the studs is 600 mm.
- 140 mm fibreglass;
- 15 mm gypsum;
- The inside and outside surface convection coefficients h_{int} and h_{ext} are assumed 8 and 34 W/m^2.K respectively;
- The wall is 2.5 m high and 1.24 m wide.

For this study, the calculations have been carried out for constant outside conditions, with a sol-air temperature of -20 ^{0}C and an interior air temperature of +20 ^{0}C. The air leakage comes in through cavity Cav0 at -20 ^{0}C.
To study the effect of the cavity opening positions through the wall, the following scenarios were proposed (see arrows in Figure 1):

- **SC0**: Infiltration through cavity Cav0 across the whole wall thickness.
- **SC1**: Infiltration through cavities Cav0, Cav1, Cav6, Cav10 and Cav0.
- **SC2**: Infiltration through cavities Cav0, Cav1, Cav2, Cav3, Cav8, Cav12, Cav11, Cav10 and Cav0.
- **SC3**: through cavities Cav0, Cav1, Cav2, Cav3, Cav4, Cav9, Cav13, Cav12, Cav11, Cav10 and Cav0.

Cavities are 3 mm thick. The airflow rate is assumed 0.005 kg/s.
Heat flux on the interior and exterior surfaces is calculated by the numerical method at every time step as follows:

$$Q_{int} = \frac{h_{int}}{N} \sum_{i=1}^{N} (T_{int\_wall\_side} - T_{int})_i \quad (9)$$

$$Q_{ext} = \frac{h_{ext}}{N} \sum_{i=1}^{N} (T_{ext} - T_{ext\_wall\_side})_i \quad (10)$$

$T_{int\_wall\_side}$: temperature on the interior wall surface.
$T_{ext\_wall\_side}$: temperature on the exterior wall surface.
N: number of nodes i.

Figure 4 shows the increase of air temperature from the inlet point (Cav0 on the outer surface) to the outlet (Cav0 on the inner surface) with the leakage route length (L).
With the scenario SC0, the air leakage would take the short cut leading to the interior side of the room. The heat exchange surface between the mass of air and the wall components is restricted to the wall thickness. At the outlet (the inner side of the wall), the air recovered 5^{0}C. With longer leakage routes (for instance scenario SC1), the temperature difference of the flowing air between the inlet and the outlet is about 7.5^{0}C. This heat recovery phenomenon increases significantly with scenarios SC2 and SC3 where the air temperature variations through the cavities are visibly more pronounced.

As shown in Figure 4, the average heat loss through the wall is a function of the air leakage route length, varying from 17.70 W/m^2 for the shortest path SC0, to 63.24 W/m^2 for the longest one SC3.

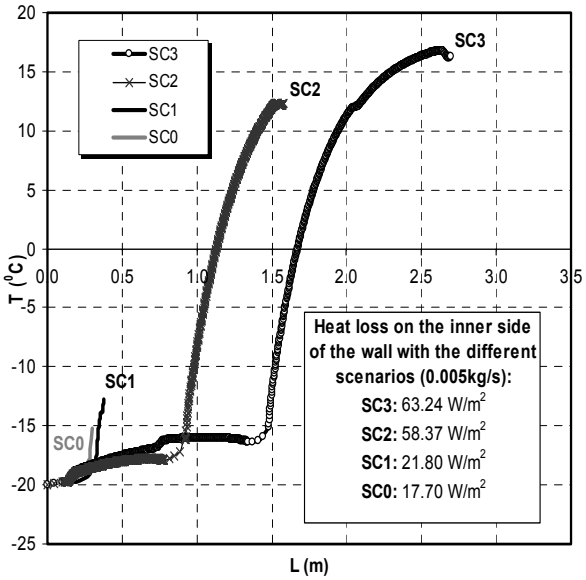

Figure 4: Air temperature progression inside the cavities with the different scenarios

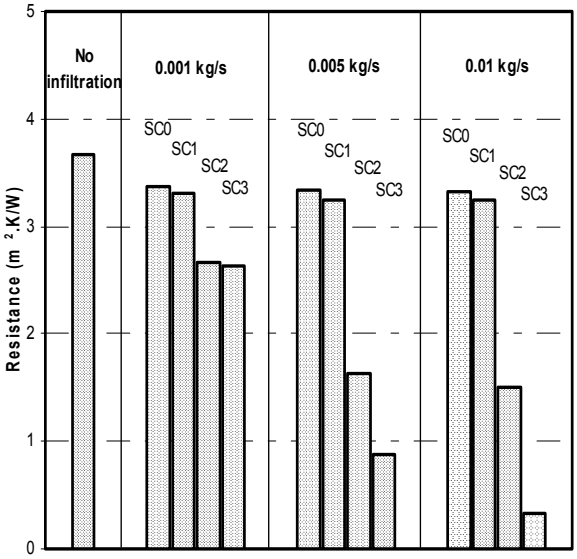

Figure 5: Wall thermal resistance with different scenarios and airflow rates

Combined effect of the airflow rates and leakage routes on the wall performance

The airflow rate is a significant parameter affecting the thermal wall performances. The four scenarios (SC0, SC1, SC2 and SC3) described earlier were used with different airflow rates (0.001, 0.005 and 0.01 kg/s).

The studs (layer ❻) cause thermal bridging in the wall system, and as a consequence of the air infiltrating through the cavities, the heat flow is bi-dimensional (in OX and OZ directions) across the thickness of the wall.

To study the effect of the air leakage route on the wall system performances, the thermal resistance R_{wall} was defined as follows:

$$R_{wall} = \frac{1}{N.Q_{int}} \sum_{i=1}^{N} (T_{int\_wall\_side} - T_{ext\_wall\_side})_i \quad (11)$$

Where "N" indicates the number of nodes on the interior or exterior sides of the wall. Q_{int} (W/m^2) is the average heat flux calculated at the interior surface (Equation 9).

When the airflow enters the wall and travels through cavities (according to the leakage route) before entering the house, the overall wall resistance is degraded. Figure 5 evaluates the effect of the washing air on R_{wall} with different scenarios and airflow rates.

With relatively short leakage routes (scenarios SC0 and SC1), the overall resistance is not significantly affected by the airflow rate. Compared to the wall without any infiltration, R_{wall} is reduced by about 9%.

With longer leakage routes (SC2 and SC3), the overall resistance is degraded significantly (decreasing by about 30% to 90%).

The heating load of a building could be divided into:

- Heat loss through the wall system (Q_{int}).
- Heating load required to heat the air infiltration entering the house ($M.C_p.\Delta T$), which can account according to the literature of up to 50% to 60% of the total space load.

Figure 6 illustrates the heating load at different scenarios and airflow rates. Comparing the cases with and without infiltration, the results show the significant effect of the air intrusion on the total heating load. For instance, an increase of about 100% is noticed with scenario SC3 and a rate of 0.001 kg/s.

The heat recovery factor, ε, as introduced by Claridge and Bhattacharya to account for all of the thermal interaction between leaking air and building walls, including the effect on conductive heat loss, is calculated as follows (Claridge et al., 1990):

$$\varepsilon = 1 - \frac{(Q - Q_0).A}{M.Cp.\Delta T} \quad (12)$$

Q (W/m^2): is the total heating load considering the coupling between heat and air transfer ($Q = Q_{int}$ + Heating load due to infiltration); Q_0: is the conduction load when there is no infiltration (10.98 W/m^2 for this wall); ΔT is the temperature difference between inside and outside (40^{0}C); M is the mass flow rate of infiltrated air (kg/s); A is the wall area.

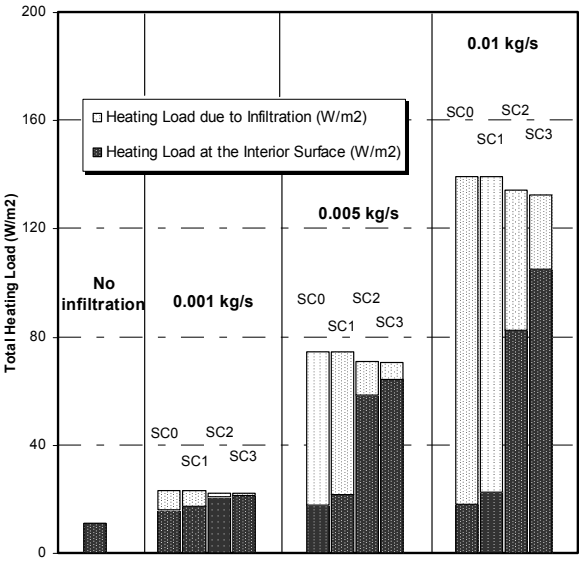

Figure 6: Heating load at different scenarios and airflow rates

Table 1 shows the heat recovery factor, ε, at different scenarios and airflow rates. With the three airflow rates tested during this study, the total heating load is reduced for longer air leakage route (SC2 and SC3).

Table 1: Heat recovery factor at different scenarios and airflow rates

Scenario (Path (kg/s))	Q (W/m^2)	M.Cp.ΔT/A (W/m^2)	ε (%)
SC0 (0.001)	22.97	12.90	7.1
SC1 (0.001)	22.89	12.90	7.7
SC2 (0.001)	22.27	12.90	12.5
SC3 (0.001)	21.97	12.90	14.8
SC0 (0.005)	74.62	64.52	1.3
SC1 (0.005)	74.59	64.52	1.4
SC2 (0.005)	70.74	64.52	7.4
SC3 (0.005)	70.53	64.52	7.7
SC0 (0.01)	139.06	129.03	0.7
SC1 (0.01)	139.05	129.03	0.8
SC2 (0.01)	134.59	129.03	4.2
SC3 (0.01)	132.47	129.03	5.8

Cold air recovers heat all the way long before reaching gradually the inner side temperature. With the air leakage routes SC0 and SC1, a shortcut is created between the exterior and the interior sides of the wall, resulting in a less effective heat exchanger. The heat recovery is significant with an airflow rate of 0.001 kg/s as the factor ε takes values between 7% and 15%. Lower rates, which can occur in energy efficient houses, might lead to higher heat recovery factor ε.

When the overall heating load is evaluated with the steady-state conventional method, the heat loss (Q_0) through the wall system is underestimated (since the effect of air infiltration on the heating load at the interior surface is neglected), and the heating load required to heat the infiltrated air entering the house is overestimated (when neglecting the heat recovery through the wall layers). To characterize the actual air leakage effect on the wall performance, the overall heating load calculated numerically ($Q= Q_{int}$ + Heating load due to infiltration) was compared to the one calculated with the steady-state conventional method $[Q_0+(MCp(T_{int}-T_{ext}).A^{-1})]$. The Reduction of Heating Load (RHL) is defined as:

$$RHL=[Q-(Q_0+MCp(T_{int}-T_{ext})A^{-1}]/(Q_0+MCp(T_{int}-T_{ext})A^{-1}] \quad (13)$$

RHL is presented in Figure 7 at different scenarios and airflow rates. The reduction was significant for long airflow paths (SC2 and SC3), varying between 4% and 8%.

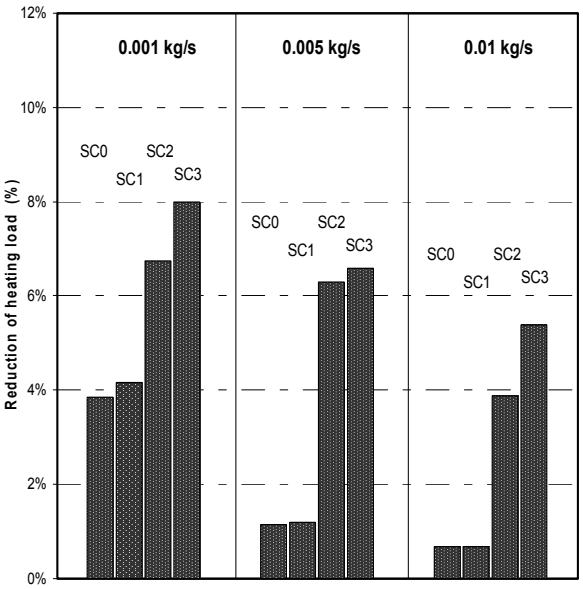

Figure 7: The overall reduction of heating load at different scenarios and airflow rates

CONCLUSIONS AND FUTURE WORK

The results show the significant effect of airflow on the thermal performance of the wall. Heating load is evaluated depending on the air leakage route and the airflow rate. The wall behaves as a heat exchanger. In the case of air flowing at a rate of 0.001 kg/s through the cavities, the heat recovery factor, ε, has values between 7 % and 15% depending on the flow path. For the different scenarios and airflow rates tested, the reduction of heating load reaches 8%.

In future work, the calculation of air mass flow rate in terms of a given pressure difference (between outside and inside) and physical characteristics of air cavities (thickness, length, etc.), will be implemented in the

code. Typical airflow rates in wall cavities will be tested. The case of exfiltration will be also examined. The air intrusion through the insulation pores will be proposed to be added to the model including the moisture effect that causes heat loss coefficient degradation. The numerical simulation will be validated by an experimental work.

ACKNOWLEDGEMENTS

The authors acknowledge the support received from the Natural Sciences and Engineering Research Council of Canada.

REFERENCES

Anderlind, G. 1985. "Energy consumption due to air infiltration",ASHRAE/DOE/BTECC Conference on Thermal Performance of the Exterior Envelopes of Buildings, Clearwater Beach, FL, pp. 201-208.

ASHRAE Fundamentals, 1993.

ASHRAE Fundamentals, 2001, Chapter 25.

Bhattacharyya, S., Claridge, D.E. 1995. "The Energy Impact of Air Leakage Through Insulated Walls", Journal of Solar Energy, Vol. 117, pp. 167-172.

Brown, W.C., Bomberg, M. T., Ullett, J.M. 1993. "Measure Thermal Resistance of Frame Walls with Defects in the Installation of Mineral Fiber Insulation.", J. Thermal Insulation and Building Environmnents., Vol. 16, pp.318-339.

Chebil, S., Galanis, N., Zmeureanu, R. 2002. "Computer simulation of air infiltration effects on heat transfer in multilayered walls", eSim2002 Conference, Montreal, pp.97-104.

Claridge, D.E., Bhattacharyya, S. 1990. The measured impact of infiltration in a test cell, J. Solar Energy Engineering, Vol.117, pp.167-172.

Claridge, D.E., Liu, M. 1996. "The Measured Energy Impact of Infiltration in an Outdoor Test Cell", Transactions of the ASME, Vol. 118, pp.162-167.

FEMLAB User's Guide and Introduction, Version 2.2, Copyright 2001 by COMSOL AB.

Hollands K.G.T., Konicek L. 1973. "Experimental Study of the Stability of Differentially Heated Inclined Air Layers", Int. J. Heat Mass Transfer, Vol. 16, pp. 1467-1476.

Jakob, M. 1949. Heat Transfer Vol.1, Wiley NY.

Jones, D.C., Ober, D.G., Goodrow, J.T. 1995. "Thermal Performance Characterization of Residential Wall Systems Using a Calibrated Hot Box with Airflow Induced by Differential Pressures", Airflow Performance of Building Envelopes, Components and Systems, ASTM STP 1255, American Society for Testing and Materials, Philadelphia, pp.197-228.

Kohonen, R., Virtanen, M. 1987. "Thermal coupling leakage flow and heating load of buildings". ASHRAE Transactions, Vol. 93, pp. 2303-2318.

Krarti, M. 1994. "Effect of Air Flow on Heat Transfer in Walls", Journal of Solar Energy, Vol. 116, pp. 35-42.

Liu, M. 1987. "Thermal techniques in buildings", Harbin Architectural and Civil Engineering Institute Press, Harbin, China.

Patankar, S.V. 1980. Numerical Heat Transfer and Fluid Flow, Hemisphere Publishing Corporation.

Powell, F., Krarti, M., Tuluca, A. 1989. "Air Movement Influence on the Effective Thermal Resistance of Porous Insulation: A Literature Survey", Journal of Thermal Insulation, Vol. 12, pp. 239-251.

Sherman, M.H., Walker, I.S. 2000. "Heat Recovery in Building Envelopes", ASHRAE/DOE/BTEC Thermal Performance of the Exterior Envelopes of Buildings VIII, ASHRAE, Atlanta, GA.

NOMENCLATURE

Cp	Specific heat (J/kg.K)
D_h	Hydraulic diameter (m)
Gr	Grashof number
h	Convection coefficient ($W/m^2.K$)
H	Height (m)
i,j,k	i-th, j-th, k-th node on OX, OY and OZ directions, respectively
I	Solar radiation (W/m^2)
k	Thermal diffusivity (m^2/s)
K	Thermal conductivity (W/m.K)
M	Mass flow rate of infiltrated air (kg/s)
n, p	n-th, p-th element
Pr	Prandtl number
Q	Heat flux (W/m^2)
Re	Reynolds number
T	Temperature (^0C)
t	Time (s)
T_{ext}	Sol-air temperature at the outside surface (^0C)
T_{int}	Interior air temperature (^0C)
T_m	Mean temperature of two boundary facing surfaces (^0C)
T_{out}	Exterior air temperature (^0C)
T^t	Temperature at time t (^0C)
x,y,z	Cartesian coordinates
α	Absorptivity coefficient
β	Temperature coef. of volume expansion (1/K)
Δ	Time or distance increment
δ	Gap/cavity thickness (m)
ε_{eff}	Effective emissivity
ν	Cinematic viscosity (m^2/s)
ρ	Density (kg/m^3)
σ	Stefan-Boltzmann constant ($W/m^2.K^4$)